Journal of Pharmacokinetics and Biopharmaceutics, Vol. 17, No. 6, 1989

Hepatic Modeling of Metabolite Kinetics in Sequential and Parallel Pathways: Salicylamide and Gentisamide Metabolism in Perfused Rat Liver

Xin Xu[1] and K. Sandy Pang[1-3]

Received November 23, 1988—Final September 14, 1989

Previous data on salicylamide (SAM) metabolism in the perfused rat liver had indicated that SAM was metabolized by three parallel (competing) pathways: sulfation, glucuronidation, and hydroxylation, whereas sequential metabolism of the hydroxylated metabolite, gentisamide (GAM), was solely via 5-glucuronidation to form GAM-5G. However, under comparable conditions, preformed GAM formed mainly two monosulfate conjugates at the 2- and 5-positions (GAM-2S and GAM-5S); 5-glucuronidation was a minor pathway. In the present study, the techniques of normal (N) and retrograde (R) rat liver perfusion with SAM and mathematic modeling on SAM and GAM metabolism were used to explore the role of enzymic distributions in determining the dissimilar fates of GAM, as a generated metabolite of SAM or as preformed GAM. Changes in the steady-state extraction ratio of SAM (E) and metabolite formation ratios between N and R perfusions were used as indices of the uneven distribution of enzyme activities. Two SAM concentrations (134 and 295 μM) were used for single-pass perfusion: the lower SAM concentration exceeded the apparent K_m for SAM sulfation but was less than those for SAM glucuronidation and hydroxylation; the higher concentration exceeded the apparent K_m's for SAM sulfation and glucuronidation but was less than the K_m for hydroxylation. Simulation of SAM metabolism data was carried out with various enzyme distribution patterns and extended to include GAM metabolism. At both input concentrations, E was high (0.94 at 134 μM and 0.7 at 295 μM) and unchanged during N and R, with SAM-sulfate (SAM-S) as the major metabolite and GAM-5G as the only detectable metabolite of GAM. Saturation of SAM sulfation occurred at the higher input SAM concentration as shown by a decrease in E and a proportionally less increase in sulfation rates and proportionally more than expected increases in SAM hydroxylation and glucuronidation rates. At both SAM concentrations, the steady-state ratio of metabolite formation rates for SAM-S/SAM-G decreased when flow direction changed from N to R. An insignificant decrease in SAM-S/SAM-OH was observed at the low input SAM

This work was presented in part at the ASPET meeting, Montreal, 1988, and was conducted in partial fulfilment of Xin Xu's Ph.D. thesis. This work was supported by the Medical Research Council of Canada and a grant from the Canadian Liver Foundation.

[1]Faculty of Pharmacy, University of Toronto, Toronto, Ontario, Canada M5S 2S2.

[2]Department of Pharmacology, Faculty of Medicine, University of Toronto, Toronto, Ontario, Canada M5S 1A1.

[3]To whom correspondence should be addressed at Faculty of Pharmacy, 19 Russell Street, University of Toronto, Toronto, Ontario, Canada M5S 2S2.

0090-466X/89/1200-0645$06.00/0

concentration, due to the small amount of SAM-OH formed and hence large variation in the ratio among the preparations, whereas at the high input SAM concentration, the decrease in SAM-S/SAM-OH with a change in flow direction from N to R was evident. The metabolite formation ratio, SAM-G/SAM-OH, however, was unchanged at both input concentrations and flow directions. The observed data suggest an anterior SAM sulfation system in relation to the glucuronidation and hydroxylation systems, which are distributed similarly. When the observations were compared to predictions from the enzyme-distributed models, the best prediction on SAM metabolism was given by a model which described sulfation activities anteriorly, glucuronidation activities evenly, and hydroxylation activities posteriorly (perivenous). When the model was used to predict data for SAM and GAM metabolism in once-through perfused rat livers at different input SAM concentrations, in the absence or presence of the sulfation inhibitor, 2,6-dichloro-4-nitrophenol (DCNP), the predictions were in close agreement with previously observed SAM data but failed to predict the exclusive formation of GAM-5G; rather, GAM-2S and GAM-5S were predicted as major sequential metabolites of SAM. The poor correlation for GAM metabolic data may be explained on the basis of subcellular enzyme localizations: the cytochromes P-450 and UDP-glucuronyltransferases, being membrane-bound enzymes, are more coupled for GAM formation and glucuronidation, when GAM was generated intracellularly. The present study suggests that subcompartmentalization of enzymes may need to be considered in hepatic modeling for better prediction of metabolic events.

KEY WORDS: Hepatic modeling; parallel and sequential metabolism; metabolite kinetics; normal and retrograde liver perfusion; hepatic enzymatic distribution; salicylamide; gentisamide; sulfation; glucuronidation; hydroxylation.

INTRODUCTION

The manner in which competing metabolic pathways exert their influence on one another in the liver has been studied both theoretically (1,2) and experimentally (3–8). In a well-mixed system such as hepatocytes or liver homogenates, substrate removal tends toward the high-affinity, low-capacity pathways, and by virtue of depletion of substrate, these high-affinity, low-capacity pathways preclude formation of metabolites from low-affinity, high-capacity pathways. The low-affinity pathways become important metabolic pathways only upon substrate loading and saturation of the high-affinity pathways (9,10). In the intact liver, however, enzymes for high- and low-affinity pathways are regionalized within the liver acinus. Drug elimination therefore must be examined with respect to zonation of enzymes, their apparent kinetic constants, and the microcirculation. Uptake and metabolism of drugs occur along the direction of flow of substrate and processing of a drug at any point along the sinusoidal flow path is influenced by elimination processes preceding or at that point. Hence, competing pathways exert their influence by modulating the intrahepatic substrate concentration. When a high-affinity pathway is concentrated within upstream hepatocytes, it will efficiently prevent substrate recruitment for hepatocyte activities further downstream. This effect is greatest at low substrate concentrations entering the liver, where the change in intrahepatic concentrations is the greatest.

In sequential pathways where a drug is metabolized solely to a primary and then a secondary metabolite, the presence of the primary metabolite is dependent on the extent of drug uptake and biotransformation. Preformed (primary) metabolite (one which is entering the liver as an already formed entity), however, is itself subject to uptake and biotransformation or excretion. Albeit the same enzyme system(s) and uptake process(es) are responsible for the elimination of both preformed and generated metabolites, differences are expected because of their different points of entry in the liver. For example, in the case where the enzymic system for formation and metabolism of the primary metabolite are distributed evenly, as in a well-mixed system for isolated hepatocytes (11) or in an intact liver (12), metabolism of the generated metabolite generally "lags" behind that of preformed metabolite. This kinetic phenomenon is due to the nature of drug and metabolite processing, that a delay exists for the generated metabolite in comparison to the preformed metabolite (13). Differences in the enrichments and distribution of enzymes for formation and metabolism of the primary metabolite will result in further differences (14), as exemplified in phenacetin *O*-deethylation to acetaminophen followed by acetaminophen sulfation. The perihepatic venous enrichment of *O*-deethylation activity and the periportal preponderance of sulfation activity render reduced sulfation of acetaminophen, when generated from phenacetin, in comparison to that of preformed acetaminophen during a single passage of both preformed acetaminophen and phenacetin through the liver (15,16). Zonal distribution of enzymes can therefore significantly influence the disappearance of the parent compound as well as the formation of metabolite(s) in both parallel and sequential pathways.

Recently, parallel and sequential metabolic pathways have been examined simultaneously for salicylamide (SAM) (17). This substrate is removed by three competing pathways in the perfused rat liver. It is predominantly sulfated by a high-affinity, high-capacity pathway to SAM-S (SAM sulfate conjugate). Upon high substrate loading and saturation of sulfation pathway, SAM is glucuronidated by a lower-affinity but high-capacity pathway to SAM-G (SAM glucuronide conjugate). A third and minor pathway is the hydroxylation of SAM (low-affinity, low-capacity pathway) at the 5-position to form gentisamide (GAM), which is further metabolized solely to form GAM-5-glucuronide (GAM-5G) (18). However, under comparable GAM concentrations, preformed GAM is primarily sulfated at 2- and 5-positions to form gentisamide 2-sulfate (GAM-2S) and gentisamide 5-sulfate (GAM-5S) and is glucuronidated to form GAM-5G only upon GAM loading into the liver and saturation of the higher-affinity sulfation pathways (5). The astounding difference in GAM metabolism between SAM and GAM administration may be explained by difference in

enzyme distributions for conjugate formation. It is possible that perhaps hydroxylation activity of SAM is enriched downstream and is more coupled with GAM glucuronidation activities (6).

The present study examined the zonal distributions of enzyme activities in the metabolism of salicylamide (SAM) to explain the exclusive formation of GAM-5G after SAM administration. The technique of normal and retrograde liver perfusions was used to assess the extent of SAM metabolite formation upon a change in SAM input concentration or direction of flow. The observed data and previous data on SAM metabolism (17) in the absence or presence of a sulfation inhibitor, 2,6-dichloro-4-nitrophenol (DCNP), were compared with predictions from enzyme-distribution models. The enzyme kinetic parameters K_m and V_{max} previously determined for SAM sulfation, glucuronidation, and hydroxylation (19) and for GAM sulfation and glucuronidation (6) were used in the predictions.

MATERIALS AND METHODS

Materials. Male Sprague-Dawley rats were purchased from Charles River (St. Constant, Canada). SAM was obtained from Sigma (St. Louis, MO). ^{14}C-SAM (sp act, 6.82 mCi/mmol) was synthesized according to Mandel *et al.* (20). The purity of ^{14}C-SAM used for perfusion studies was greater than 99%, as found by TLC and HPLC. All other solvents for chromatography were of glass-distilled HPLC grade (Burdick and Jackson, Muskegon, MI), and other chemicals were of analytical grade.

Liver Perfusion. The surgical procedure and the perfusion apparatus were identical to those previously described (17). Male Sprague-Dawley rats (320–416 g) were used as liver donors. The liver weights at the end of the experiments were determined to be 8.2–12.6 g. The perfusion medium consisted of 20% washed human red blood cells (Red Cross, Toronto), 1% bovine serum albumin (Sigma Chemical Co., St. Louis, MO), and 300 mg/100 ml of glucose in Krebs-Henseleit bicarbonate solution buffered to *p*H 7.4. Perfusate was delivered at a constant flow rate (10 ml/min/liver) once through the rat liver preparation by either normal (N) or retrograde (R) flow direction. Preliminary experiments indicated that steady state for SAM elimination was achieved within 20 min in both N and R perfusions. Each liver perfusion study consisted of three experimental periods: the first and second periods were of 40-min duration, whereas the third period was of 60-min duration. Perfusion was started with either normograde or retrograde flow in the first period, then switched to the opposite direction in the second period, and finally switched again during the third period such that the first and last periods had the same flow direction. Since R perfusion for long periods of time reduces liver function, most studies were conducted

with the design, NRN. Control experiments perfused in RNR order were also performed. The viability of each preparation was checked by continuously monitoring SGOT level during entire perfusion periods. Because slight deterioration of the liver was observed in the last period, the average metabolic data in the first and the last periods were used to compare with that in the second period.

Two sets of experiments were performed to investigate the effects of input concentration and flow direction on the metabolism of SAM. In the first group of four experiments lower concentrations of SAM (101–177 μM, 7×10^4 dpm/ml) were used, while higher concentrations (241–381 μM, 7.5×10^4 dpm/ml) were employed in the second series of six experiments. The choice of the concentrations is based on simulation results from a previous theoretical study: the relative ratio between input substrate concentration and K_m of enzyme will influence the sensitivity of model differentiation (1). The average concentration (134 μM) of the first set of experiments exceeded the apparent K_m for SAM sulfation but was less than those for SAM glucuronidation and hydroxylation. The mean value (295 μM) of the second group of experiments was greater than the apparent K_m's for SAM sulfation and glucuronidation but less than the K_m for hydroxylation.

Two samples were taken from the reservoir to determine the steady-state input concentrations. Outflow samples were collected during the last 20 min of each perfusion period; five samples were taken at 4-min intervals. Bile samples were collected *in toto* at 0–20, 20–25, 25–30, 30–35, and 35–40 min during the first two periods and at 0–40, 40–45, 45–50, 50–55, and 55–60 min in the last period.

Assay. SAM and its metabolites in perfusate and bile were analyzed by previously reported HPLC methods (21). An extraction procedure was used to determine SAM and GAM concentrations in perfusate (blood). Conjugates of SAM and GAM in plasma and bile were separated by a reverse-phase C_{18} column with 0.085 M KH_2PO_4 (pH 3.4) as the mobile phase which was delivered by a flow-gradient program. The peaks corresponding to SAM and SAM metabolites eluted from the HPLC column were collected, and radioactivity was counted by liquid scintillation by assuming a constant specific activity for SAM and the metabolites. Only the metabolite fractions with counts that were three times the background were treated as real peaks (21).

Data Analysis. Steady-state hepatic extraction ratio (E) of SAM was calculated by

$$E = \frac{(C_{In} - C_{Out})}{C_{In}} \tag{1}$$

where C_{In} and C_{Out} represent steady-state input and output concentration, respectively. Metabolite formation rates at steady state were determined as the sum of biliary excretion rate of the metabolite and the rate of appearance of metabolite in the perfusate:

$$v^{mi} = QC_{Out}\{mi\} + \frac{\Delta A_e\{mi\}}{\Delta t} \tag{2}$$

where v^{mi} and $C_{Out}\{mi\}$ are the steady-state formation rate and the outflow concentration for the primary metabolite mi, respectively. Q is the perfusion flow rate (10 ml/min/liver). $\Delta A_e\{mi\}/\Delta t$ represents the biliary excretion rate for mi, at steady state. It should be pointed out that Eq. (2) is valid only if the ratio of blood/plasma for the conjugate is equal to one. Apparently, the assumption is valid because the blood/plasma ratio for SAM-S was around 0.93, whereas those for GAM conjugates were around unity (unpublished data). Formation rates for unconjugated and conjugated GAM were summed to obtain the steady-state hydroxylation rate of SAM (SAM-OH). The ratios of the steady-state metabolite formation rates between various pathways, i.e., SAM-S/SAM-G, SAM-S/SAM-OH, and SAM-G/SAM-OH, were calculated for both N and R perfusions.

Modeling and Computer Simulation. Computer simulation on the distribution of enzyme activities for SAM metabolism was carried out on a Sun computer system (Sun IPC, Sun Microsystems Inc.), with a program written in FORTRAN 77. Simulations were performed to examine the effects of enzyme distribution patterns, direction of flow, and input substrate concentration on the elimination of SAM to form various metabolites. Modeling approaches were the same as those reported previously (5,6). The following assumptions were made: (a) the flow path in liver is tubular, surrounded by single sheets of hepatocytes of varying or constant enzymatic activities, (b) the system was perfusion-limited, that is, transport of SAM and GAM across membranes is rapid and not rate-limiting, (c) unbound SAM and GAM in sinusoidal blood rapidly equilibrate with those in tissue—the two unbound concentrations are equal at steady-state, (d) only the unbound species in tissue is eliminated, (e) the K_m for each metabolic pathway is constant along the flow path of length L, whereas the enzymatic activity ($V_{max,x}$) may vary at any point x along the flow path, depending on the enzyme distribution pattern, and (f) the same transport and metabolic processes are involved in the uptake and elimination of preformed and generated GAM. The overall length-averaged enzymatic activities (V_{max}) is expressed as

$$V_{max} = \int_0^L V_{max,x}\, dx/L \tag{3}$$

The simulation was approached in two parts. In the first part, three parallel competing pathways for SAM metabolism were considered (parallel model), that is, the ratios of SAM sulfation, glucuronidation, and hydroxylation (sum of formation rates of GAM and GAM-5G). The equations for SAM elimination and metabolites formation are described in Appendix A. Previous experiments had revealed nonlinear binding of SAM to albumin and that saturation of binding to one class of the binding sites (association constant, $K_1 = 1.33 \times 10^3\ M^{-1}$; the number of binding sites, $N_1 = 2.1$) occurred within the concentration range studied, that is, the unbound fraction of SAM would change during a single passage through the rat liver (19). This aspect has been taken into consideration in our simulations. Since the blood/plasma ratio of SAM is unity (19), the unbound sinusoidal plasma concentration, $C_{P,u}$, which also equalled the unbound blood sinusoidal concentration, may be estimated in terms of the constants and the total plasma concentration, C_p (19):

$$C_{p,u} = \frac{-(1 + N_1K_1[P_t] - K_1C_P) + \{(1 + N_1K_1[P_t] - K_1C_P)^2 + 4K_1C_P\}^{1/2}}{2K_1} \quad (4)$$

The enzymatic parameters used in the simulations were taken from our previous investigations on SAM metabolism in the once-through liver: values of 14.8, 151, and 281 μM for $K_m^{SAM\text{-}S}$, $K_m^{SAM\text{-}G}$, and $K_m^{SAM\text{-}OH}$ and 155, 200, and 88.7 nmol/min/g for $V_{max}^{SAM\text{-}S}$, $V_{max}^{SAM\text{-}G}$, and $V_{max}^{SAM\text{-}OH}$, respectively (19), were used. Five different enzyme distribution patterns were utilized (Fig. 1, models A to E) to describe $V_{max,x}$ for SAM sulfation and glucuronidation, as those described by Morris *et al.* (6). For SAM hydroxylation, however, an additional enzyme distribution pattern was also used (Fig. 1, model F). For the description of the three pathways, the first, second, and third letters denote that distribution pattern for SAM sulfation, glucuronidation, and hydroxylation, respectively.

Simulations were performed based on different combinations of enzyme distribution pattern for each competing pathway, resulting in $5 \times 5 \times 6$ or 150 possible combinations. Two input concentrations (140 and 300 μM) and different flow directions (normal and retrograde perfusions) were examined. The simulated results, expressed as steady-state E and formation rate ratios of SAM-S/SAM-G, SAM-S/SAM-OH, and SAM-G/SAM-OH, were compared with observed values at both concentrations and different flow directions. The least weighted sum of square of residuals between simulated and observed values was used as a criterion for selection of the best model.

In the second part of the simulation, extended enzyme models, which included the sequential metabolism of GAM to GAM conjugates (parallel-sequential models), were used. Here, the mass balance differential rate

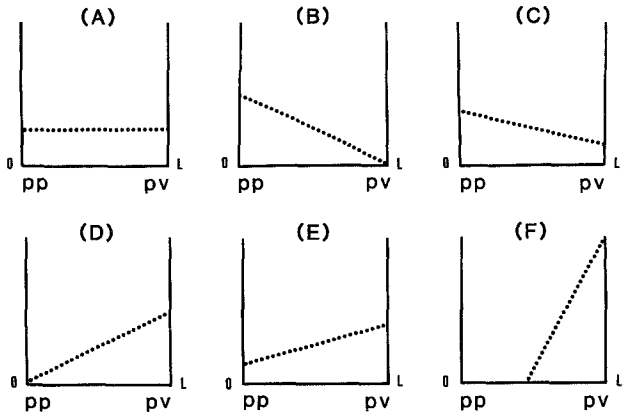

Fig. 1. Schematic representation of enzymic distribution patterns (A to F) for SAM metabolism in the liver. Total enzymatic activity (V_{max}) is assumed to be constant for each enzyme in all six patterns, while $V_{max,x}$ is varied along the sinusoidal flow path from input 0 to output L. Terminologies pp and pv represent the periportal (near the inlet) and perivenous (near the outlet) regions, respectively. Distribution Pattern A denotes an evenly distributed system; Pattern B denotes a linear gradient, starting from high levels at the inlet, dwindling to zero at the outlet of the liver, and Pattern D is the reverse of Pattern B; Pattern C shows a high enzyme level at the inlet, with a linear decrease toward the outlet to $\frac{1}{3}$ of the original enzymic activity, and Pattern E is the reverse of Pattern C; Pattern F denotes an enzyme distribution pattern in which the enzyme is absent in the first half of the liver and increases linearly toward the outlet of the liver. The first, second, and third letters of the model denote the distribution patterns of SAM sulfation, glucuronidation, and hydroxylation activities, respectively. The fourth, fifth, and six letters of the extended-models denote GAM 2- and 5-sulfation activities and glucuronidation activities, respectively.

equations for SAM elimination and SAM-S and SAM-G formation [Appendix A, Eqs. (1A)-(A3)] were again based on removal of unbound SAM [Eq. (4)]. Since binding of GAM was concentration independent (5), the unbound concentration of GAM may be expressed in terms of the unbound fraction in blood, $f_B\{mi\} = 0.516$, multiplied by the total concentration of GAM in blood. Additional equations to describe the rate of appearance of GAM and formation of GAM-2S, GAM-5S, and GAM-5G are shown in Appendix B. The values of K_m and V_{max} for formation of GAM-2S, GAM-5S, and GAM-5G were based on published results by Morris *et al.* (5). These enzymatic constants were as follows: GAM-2S—$K_m = 22\ \mu M$, $V_{max} = 287$ nmol/min/liver; GAM-5S—$K_m = 26\ \mu M$, $V_{max} = 978$ nmol/min/liver; and GAM-5G—$K_m = 71\ \mu M$, $V_{max} = 1062$ nmol/min/liver. Since two identical, anterior enzymic distribution for 2- and 5-sulfoconjugation and a

posterior localization for 5-glucuronidation well described GAM metabolism (5), simulation for the expanded parallel-sequential model was performed by extending the 10 best enzyme distribution patterns in the parallel model to include the two best enzymatic distributions for GAM metabolism (Models AAE and CCA for 2- and 5-sulfation and 5-glucuronidation of GAM). The fourth, fifth, and sixth letters would then describe the enzyme distribution patterns for GAM 2- and 5-sulfations and 5-glucuronidation, respectively. Weighted sums of squares of residuals (WSSR) were calculated based on the difference between observed and simulated values for E, SAM-S/SAM-G, SAM-S/SAM-OH, and SAM-G/SAM-OH at both low and high input SAM concentrations with normal or retrograde perfusions. Since no GAM sulfate conjugate was detected in the liver perfusion with SAM, it was not suitable to calculate the WSSR for GAM sulfation reactions, as in this case $\{(\text{observed}-\text{predicted})^2/\text{predicted}^2\}$ equals one. The absolute differences (ADIF) between observed and simulated values for formation rates of GAM-2S, GAM-5S, and GAM-5G were calculated instead.

The 10 best parallel models (with smallest WSSR) were selected and used in the parallel-sequential models. To test the validity of the enzyme distribution patterns, the models were used to simulate data on SAM metabolism, in the absence or presence of the sulfation inhibitor DCNP (2,6-dichloro-4-nitrophenol), which were then compared to previously observed data (17).

Statistical Analysis. Because viability of the liver had varied during the experiment, observations during the first and last periods were averaged and compared to those in the second period using a paired t test. A P value of 0.05 was viewed as significant. The observed parameters E, steady-state sulfation, glucuronidation, and hydroxylation rates of SAM, and ratios of metabolite formation rates (SAM-S/SAM-G, SAM-S/SAM-OH, and SAM-G/SAM-OH) during the first and last periods were averaged and compared to those in the second period.

RESULTS

Normal and Retrograde Perfusion of SAM. At low input concentrations (101-177 μM), SAM was highly metabolized by the rat liver in both N and R flow directions, with E values greater than 0.94 and unchanged between N and R perfusions (Table I). SAM sulfation was the major metabolic pathway during N, which was significantly decreased during R. The minor pathways, glucuronidation and hydroxylation ($\frac{1}{4}$ and $\frac{1}{13}$ that of sulfation rate, respectively, during N), were slightly but not significantly increased

Table I. Effect of Flow Directions on the Metabolism of Salicylamide when a Low Concentration of SAM Was Delivered to the Once-Through Perfused Rat Liver

Study No.	SAM input conc., C_{in} (μM)	Direction of flow	SAM extraction ratio, E	Formation rate (nmol/min/g)			Appearance rate (nmol/min/g)		Apparent extraction ratio of GAM, $E\{mi\}_{app}$ [b]	Ratio of formation rates		
				SAM-S	SAM-G	SAM-OH[a]	GAM	GAM-5G		SAM-S/ SAM-G	SAM-S/ SAM-OH[a]	SAM-S/ SAM-OH
1	151	N[c]	0.954	97.6	16.0	9.70	1.90	7.80	0.804	6.09	10.7	1.65
		R	0.954	91.4	22.0	9.99	1.84	8.15	0.816	4.15	9.14	2.21
		N	0.978	94.6	19.9	11.0	1.30	9.74	0.882	4.75	8.57	1.80
3	177	N	0.850	117	23.5	6.03	0.46	5.57	0.924	4.98	19.3	3.89
		R	0.930	108	28.7	9.77	0.18	9.59	0.983	3.76	11.0	2.94
		N	0.900	109	30.0	10.6	0.29	10.3	0.973	3.62	10.3	2.84
11	101	N	0.956	80.7	22.5	3.37	0.68	2.69	0.798	3.59	24.0	6.69
		R	0.959	66.7	26.1	8.14	0.86	7.28	0.894	2.56	8.20	3.20
		N	0.952	77.0	27.9	5.36	0.85	4.51	0.841	2.76	14.4	5.21
12	106	R	0.992	46.3	25.8	3.92	ND[d]	3.92	1.0	1.79	11.8	6.58
		N	0.983	61.9	18.1	3.17	ND[d]	3.17	1.0	3.43	19.5	5.70
		R	0.994	45.2	21.9	2.83	ND[d]	2.83	1.0	2.06	16.0	7.73
Mean	134	N	0.945	87.5	22.0	6.61	0.913	5.87	0.903	4.08	15.7	4.18
SD	±36.6		±0.048	±22.0	±4.63	±3.29	±0.626	±2.89	±0.086	±1.02	±4.77	±2.01
		R	0.959	78.0[e]	25.2	7.77	0.720	7.10	0.923	3.10[e]	10.5	3.88
			±0.026	±27.4	±2.89	±3.17	±0.833	±2.66	±0.085	±1.03	±2.47	±2.23

[a] Sum of GAM and GAM-5G.
[b] GAM-5G appearance rate/SAM hydroxylation rate.
[c] N and R denote normograde and retrograde perfusions (10 ml/min), respectively.
[d] Not detected.
[e] Statistically significant, $P = 0.05$, N *vs* R.

(based on paired t test) when flow direction changed from N to R ($\frac{1}{3}$ and $\frac{1}{10}$ that of sulfation rate, respectively). GAM-5G was the only sequential metabolite formed upon N and R perfusions of SAM. The apparent extraction ratios of GAM in the formation of GAM-5G, found by dividing the formation rate of GAM-5G by the total appearance rate of GAM and its metabolite (or the hydroxylation rate of SAM), were 0.903 ± 0.086 and 0.923 ± 0.085, respectively, and were not different between N and R perfusions. These values are comparable to those obtained from preformed gentisamide, where the extraction ratios were about 0.9 (5, 6). Around 9% of the dose (input SAM concentration × flow × perfusion time) was excreted into the bile at steady state; the radioactivities excreted into the bile as SAM-S, SAM-G, and GAM-5G were 18, 78, and 4.7% during N perfusion and 8.3, 87, and 4.4% during R perfusion, respectively.

Deterioration of liver function in the last period was observed in the present studies. The only way to overcome the instability problem was by averaging data during the first and last period for comparison to those of the second period. A decrease in the ratio of metabolic rates, SAM-S/SAM-G, was detected upon changing the flow direction from N to R (Table I and Fig. 2). A small but insignificant decrease in the metabolic ratio, SAM-S/SAM-OH, was found in R perfusion in relation to N perfusion, and large variations were observed, perhaps due to the low and variable hydroxylation rates among individual preparations. No systemic trend, however, was observed for SAM-G/SAM-OH ratio for N and R.

At high input concentrations (241–381 μM), SAM metabolism was apparently saturated as E decreased from 0.95 to about 0.7 during both N and R (Table II). Significant differences were now observed for SAM sulfation, glucuronidation, and hydroxylation rates between N and R: higher sulfation rates were found during N compared to R, whereas smaller glucuronidation and hydroxylation rates of SAM were observed during N compared to R. SAM glucuronidation rates were 53 and 74% of SAM sulfation rates during N and R, respectively, whereas SAM hydroxylation rates were 18 and 22% of SAM sulfation rates during N and R, respectively. GAM-5G was the only detected metabolite of GAM, with the apparent extraction ratio of GAM unchanged during both directional flows (0.668 during N and 0.710 during R). These values were slightly lower than those observed in comparable perfusion studies with preformed gentisamide ($E \cong 0.8$) (5,6). Less than 14% of the dose was excreted into the bile as SAM or GAM conjugates with 5% as SAM-S, 88% as SAM-G, and 7% as GAM-5G in N, and similar results were observed in R. The statistical comparison of data between N and R indicated that the metabolite ratios of SAM-S/SAM-G and SAM-S/SAM-OH were significantly lower in R than in N, suggesting an anterior sulfation system (Fig. 3). However,

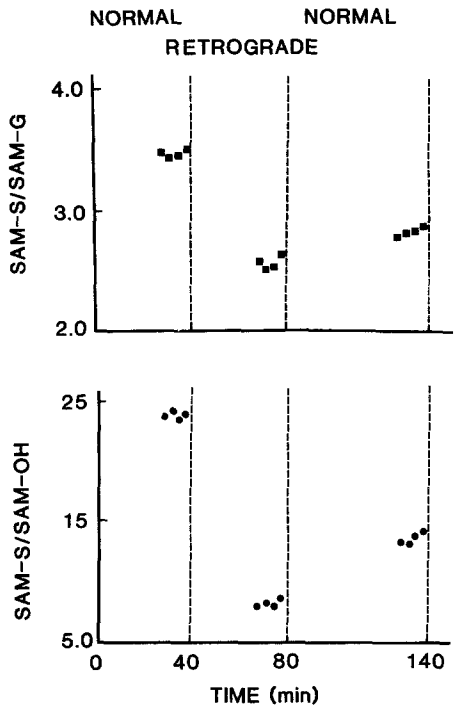

Fig. 2. A comparison of steady-state ratios of metabolite formation rates (SAM-S/SAM-G and SAM-S/SAM-OH) between normal and retrograde perfusions at 130 μM. The observations were made at steady state during each perfusion period.

SAM-G/SAM-OH were unchanged during N and R, suggesting close or parallel distribution patterns for SAM glucuronidation and hydroxylation activities.

Comparison of SAM Metabolism at 134 *and* 295 μM. The metabolic data on SAM metabolism at low (134 μM) and high (295 μM) SAM input concentrations into the rat livers were compared. Saturation of SAM metabolism was evident at the higher input SAM concentration, as the extraction ratio decreased from 0.94 to 0.7. Despite the 2.2-fold higher SAM input concentration, SAM sulfation rate failed to show the proportionate increase; sulfation rates were only 1.22- and 1.26-fold those at low input SAM concentration during N and R, respectively; SAM glucuronidation rates increased comparably by 2.6- and 2.8-fold, and SAM hydroxylation rates

Table II. Effect of Flow Directions on the Metabolism of Salicylamide when a High Concentration of SAM Was Delivered to the Once-Through Perfused Rat Liver

Study No.	SAM input conc., C_{in} (μM)	Direction of flow	SAM extraction ratio, E	Formation rate (nmol/min/g)			Appearance rate (nmol/min/g)		Apparent extraction ratio of GAM, $E\{mi\}_{app}$[b]	Ratio of formation rates		
				SAM-S	SAM-G	SAM-OH[a]	GAM	GAM-5G		SAM-S/ SAM-G	SAM-S/ SAM-OH[a]	SAM-G/ SAM-OH
2	256	N[c]	0.65	95.8	39.3	21.1	7.69	13.4	0.635	2.44	4.55	1.86
		R	0.58	72.8	43.2	22.4	8.84	13.6	0.606	1.69	3.24	1.93
		N	0.65	82.2	44.2	27.8	7.69	20.1	0.723	1.86	2.96	1.59
7	312	N	0.74	147	44.8	13.3	4.31	8.96	0.675	3.28	11.1	3.37
		R	0.75	131	57.7	23.9	3.94	20.0	0.835	2.26	5.44	2.40
		N	0.74	138	49.6	24.8	4.43	20.4	0.822	2.78	5.57	2.00
8	241	N	0.69	79.0	41.0	10.2	3.58	6.57	0.647	1.93	7.78	4.04
		R	0.59	59.0	42.5	10.7	2.89	7.77	0.729	1.39	5.54	3.98
		N	0.65	72.4	45.6	12.0	3.79	8.21	0.684	1.59	6.03	3.80
10	381	N	0.55	109	70.7	6.77	1.20	5.57	0.823	1.55	16.2	10.5
		R	0.52	93.9	89.3	17.8	0.84	17.0	0.953	1.05	5.26	5.0
		N	0.57	113	76.4	16.3	1.26	15.0	0.923	1.48	6.96	4.69
13	291	N	0.80	109	60.9	21.5	8.84	12.7	0.590	1.79	5.06	2.83
		R	0.78	84.8	74.6	24.0	8.94	15.1	0.628	1.14	3.53	3.11
		N	0.79	86.9	68.4	20.6	8.18	12.4	0.603	1.27	4.22	3.32
14	290	R	0.76	115	98.6	29.1	14.3	14.8	0.509	1.17	3.96	3.38
		N	0.77	128	71.7	25.6	14.0	11.6	0.453	1.78	4.99	2.80
		R	0.79	128	98.6	30.8	15.3	15.5	0.503	1.30	4.16	3.20
Mean	295	N	0.70	107	57.0	18.8	7.02	12.2	0.668	1.96	6.69	3.63
SD	±49.3		±0.09	±24.9	±15.6	±6.26	±5.24	±3.29	±0.141	±0.57	±2.90	±2.06
		R	0.68	98.0[d]	72.5[d]	21.5[d]	7.08	15.0	0.710	1.41[d]	4.76[d]	3.56
			±0.16	±28.3	±22.4	±6.57	±5.63	±4.43	±0.164	±0.44	±0.89	±0.96

[a] Sum of GAM and GAM-5G.
[b] GAM-5G appearance rate/SAM hydroxylation rate.
[c] N and R denote normograde and retrograde perfusions (10 ml/min), respectively.
[d] Statistically significant, $P = 0.05$, N *vs* R.

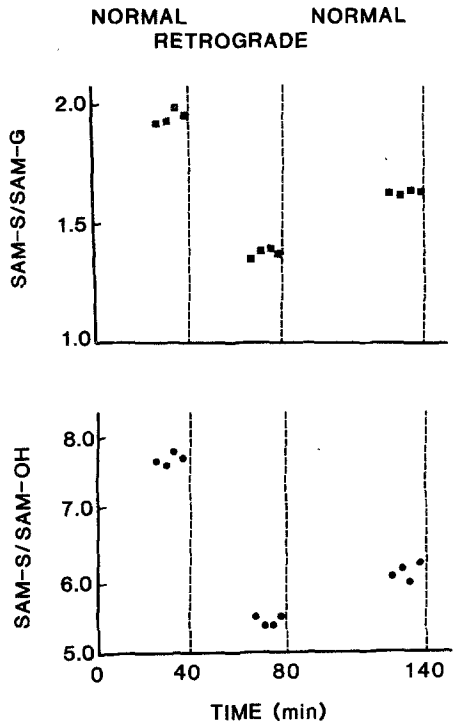

Fig. 3. A comparison of steady-state ratios of metabolite formation rates (SAM-S/SAM-G and SAM-S/SAM-OH) between normal and retrograde perfusions at 300 μM. The observations were made at steady state during each perfusion period.

by 2.8-fold during N and R, respectively, those at the low input SAM concentration. The findings suggest that saturation of SAM sulfation had occurred at the higher input SAM concentration. The apparent extraction ratio of GAM was also decreased from 0.903 ± 0.86 to 0.668 ± 0.141 during N and from 0.923 ± 0.85 to 0.71 ± 0.016 during R, suggesting that glucuronidation of GAM was apparently saturated.

The metabolic ratios of SAM-S/SAM-G, SAM-S/SAM-OH, and SAM-G/SAM-OH decreased from 4.08 to 1.96, 15.7 to 6.69, and 4.18 to 3.63, respectively, during N and from 3.1 to 1.41, 10.5 to 4.76, and 3.88 to 3.56, respectively, during R. Differences in metabolic ratios during N and R were smaller at the higher SAM input concentration (cf. Tables I and II). This observation is expected, as the intrahepatic SAM concentration gradient

was less steep during the higher input concentration, with full substrate recruitment for all metabolic activities (2).

Hepatic Modeling. One hundred and fifty combinations of enzyme distribution patterns (in parallel models) were used to described the three competing pathways in SAM metabolism. The simulated data and the weighted sums of squares of residuals for the 10 best combinations (with smallest WSSR) are listed in Table III. The following simulated results were obtained at both SAM concentrations: E was higher in R than that in N; metabolic ratios of SAM-S/SAM-G and SAM-S/SAM-OH decreased in R, and the changes in SAM-G/SAM-OH ratio, however, were variable and dependent on both the model and the flow direction. Comparatively, E decreased from low to high SAM C_{In}, and the magnitudes of change of the metabolic ratios (SAM-S/SAM-G, SAM-S/SAM-OH, and SAM-G/SAM-OH) from N to R were smaller at the high *versus* the low input SAM concentration (Table III). Because the WSSRs were very close for these models, selection of the best model could not be achieved based purely on WSSR. When the properties of the models were compared by examination of the median distances (the point of x which divides the total enzyme activity along the hepatic sinusoids into halves) for each distribution pattern, a general pattern was apparent: the median distances for sulfation < glucuronidation < hydroxylation activities for the nine best models that are all consistent with data (Table IV).

However, selection of the most appropriate model (Model CAE, BCA or AED) cannot be made due to the small statistical difference existing among model predictions. The smallest WSSR was found for Model CAE, with a decreasing pattern for SAM sulfation activities (high at inlet to one-third of inlet enzyme activity at the outlet), an even distribution for glucuronidation activities, and a posteriorly distributed SAM hydroxylation activities (increasing linearly over the length of the liver from the inlet to the outlet) (Table III). Enzymic distributions for sulfation and glucuronidation activities in this model are identical to those toward harmol (12) and gentisamide (5) and are similar to those found by other investigators for sulfation of 2-acetylaminofluorene (22,23), glucuronidation (8,24,25), and the cytochromes P-450 system (27–31).

Table V summarizes the WSSR and ADIF results for the extended, parallel-sequential models. Upon inclusion of Models CCA and AAE for GAM metabolism (6), the extended models of CCA consistently performed better than those of AAE, since smaller values of ADIF (on GAM conjugation) were observed. Based on WSSR (on SAM parameters), the combination model (Model CAECCA) gave the smallest value and was ranked as the best model. However, Model AEDCCA was found to be better in terms

Table III. A Comparison of Observed Versus Simulated Data in Parallel Models (Data from the Best 10 of 150 Models Shown)

	Low input concentration (140 μM)							
	Normal perfusion				Retrograde perfusion			
	E	SAM-S/ SAM-G	SAM-S/ SAM-OH[a]	SAM-G/ SAM-OH	*E*	SAM-S/ SAM-G	SAM-S/ SAM-OH	SAM-G/ SAM-OH
				Observations				
Mean	0.945	4.08	15.7	4.18	0.959	3.10	10.5	3.88
±SD	0.048	1.02	4.77	2.01	0.026	1.03	2.47	2.23
				Simulations				
Model								
AED	0.980	2.91	14.1	4.83	0.988	2.11	6.45	3.05
AEE	0.981	2.94	10.8	3.68	0.988	2.11	7.62	3.62
BCA	0.980	2.91	13.4	4.62	0.988	2.13	6.35	2.99
BCB	0.982	2.95	8.88	3.01	0.987	2.10	9.44	4.49
BCC	0.981	2.93	10.7	3.65	0.988	2.11	7.61	3.60
BCE	0.989	2.89	18.0	6.23	0.989	2.14	5.43	2.54
CAA	0.981	2.94	10.8	3.66	0.988	2.11	7.60	3.61
CAD	0.979	2.89	19.1	6.61	0.989	2.12	5.48	2.58
CAE	0.980	2.92	13.8	4.73	0.988	2.12	6.38	3.12
EDD	0.981	2.93	10.8	3.69	0.988	2.11	7.67	3.63

[a]Sum of GAM and GAM-5G.

Table III. Continued.

	High input concentration (300 μM)								
	Normal perfusion				Retrograde perfusion				
	E	SAM-S/ SAM-G	SAM-S/ SAM-OH[a]	SAM-G/ SAM-OH	*E*	SAM-S/ SAM-G	SAM-S/ SAM-OH	SAM-G/ SAM-OH	WSSR[b]
					Observations				
Mean	0.698	1.96	6.69	3.63	0.681	1.41	4.76	3.56	
±SD	0.088	0.57	2.90	2.06	0.116	0.48	0.89	0.96	
					Simulations				
Model									
AED	0.792	1.54	5.47	3.56	0.816	1.44	4.25	2.95	0.4985
AEE	0.795	1.55	5.04	3.26	0.813	1.43	4.28	3.21	0.5140
BCA	0.791	1.55	5.53	3.57	0.814	1.45	4.28	2.96	0.4962
BCB	0.797	1.57	4.68	2.98	0.808	1.43	4.96	3.48	0.6047
BCC	0.794	1.56	5.07	3.25	0.811	1.44	4.60	3.20	0.5028
BCE	0.788	1.53	6.06	3.95	0.817	1.46	4.00	2.75	0.5240
CAA	0.795	1.55	5.06	3.26	0.812	1.43	4.59	3.20	0.5085
CAD	0.789	1.53	6.01	3.93	0.818	1.45	3.98	2.74	0.5407
CAE	0.792	1.54	5.50	3.57	0.815	1.44	4.26	2.96	0.4874
EDD	0.795	1.54	5.03	3.26	0.814	1.42	4.56	3.21	0.5170

[a]Sum of GAM and GAM-5G.
[b]Weighted sum of squares of residuals from both low and high concentrations of SAM (1/predicted^2 was used for weighting).

Table IV. Calculated Medians of Enzymic Distributions for Salicylamide Metabolic Pathways[a]

Models	Relative enzyme location (median distance from inlet of liver)		
	Sulfation	Glucuronidation	Hydroxylation
CAE	0.382	0.5	0.618
BCA	0.293	0.382	0.5
AED	0.5	0.618	0.707
BCC	0.293	0.382	0.382
CAA	0.382	0.5	0.5
AEE	0.5	0.618	0.618
EDD	0.618	0.707	0.707
BCE	0.293	0.382	0.618
CAD	0.382	0.5	0.707
BCB	0.293	0.382	0.293

[a] Models have been ranked in decreasing order of consistency with data.

of the smallest ADIF (based on GAM conjugates). At present, no suitable statistical analysis could be performed to differentiate these models.

Upon simulation of data with use of Models CAECCA and AEDCCA and SAM input concentrations similar to those used in this study, GAM-2S and GAM-5S were predicted to be metabolites after SAM perfusion despite the fact that no GAM sulfate conjugates were observed experimentally (Table VI). The validity of the models was further tested to predict SAM metabolite formations in previous studies of the once-through liver perfusion, in which SAM input concentrations were varied stepwise, with or

Table V. Summary of WSSR and ADIF from Parallel-Sequential Models

Model	WSSR[a]	ADIF[b]
AEDCCA	0.498	64.4
AEDAAE	0.498	65.6
AEECCA	0.514	65.7
AEEAAE	0.514	66.7
BCACCA	0.496	67.9
BCAAAE	0.496	68.0
CAACCA	0.508	67.3
CAAAAE	0.508	67.7
CAECCA	0.487	66.4
CAEAAE	0.487	67.1

[a] Weighted sum of squares of residuals from both low and high concentration studies ($1/\text{predicted}^2$ was used for weighting).
[b] Absolute difference among observed and simulated values for GAM conjugates.

Table VI. A Comparison of Observed and Simulated Data from Parallel-Sequential Models

	Normal perfusion						
	E	SAM-S/ SAM-G	SAM-S/ SAM-OH[a]	SAM-G/ SAM-OH	GAM-2S[b]	GAM-5S	GAM-5G
			Low input concentrations (140 μM)				
			Observations				
Mean	0.945	4.08	15.7	4.18	0	0	5.87
±SD	0.048	1.02	4.77	2.01			2.89
			Simulations				
Model							
AEDCCA	0.980	2.91	14.1	4.83	0.95	2.74	1.29
AEECCA	0.981	2.94	10.8	3.68	1.37	3.96	1.72
BCACCA	0.980	2.91	13.4	4.62	1.27	3.65	1.44
CAACCA	0.981	2.94	10.8	3.66	1.51	4.37	1.77
CAECCA	0.980	2.92	13.8	4.73	1.13	3.25	1.37
			High input concentration (300 μM)				
			Observations				
Mean	0.698	1.96	6.69	3.63	0	0	12.2
±SD	0.088	0.57	2.90	2.06			3.29
			Simulations				
AEDCCA	0.792	1.54	5.47	3.56	2.50	7.33	3.94
AEECCA	0.795	1.55	5.04	3.26	3.21	9.38	4.64
BCACCA	0.791	1.55	5.53	3.57	3.42	9.99	4.57
CAACCA	0.795	1.55	5.06	3.26	3.66	10.7	4.97
CAECCA	0.792	1.54	5.50	3.57	3.00	8.75	4.27

[a] Sum of GAM and GAM conjugates.
[b] Formation rates for GAM conjugates (nmol/min/g).

Table VI. Continued.

	Retrograde perfusion						
	E	SAM-S/ SAM-G	SAM-S/ SAM-OH	SAM-G/ SAM-OH	GAM-2S	GAM-5S	GAM-5G
			Low input concentrations (140 μM)				
			Observations				
Mean	0.959	3.10	10.5	3.88	0	0	7.1
±SD	0.026	1.03	2.47	2.23			2.66
			Simulations				
Model							
AEDCCA	0.988	2.11	6.45	3.05	2.38	6.92	3.12
AEECCA	0.988	2.11	7.62	3.62	2.04	5.90	2.60
BCACCA	0.988	2.13	6.35	2.99	2.35	6.81	2.83
CAACCA	0.988	2.11	7.60	3.61	2.01	5.81	2.44
CAECCA	0.988	2.12	6.38	3.12	2.38	6.90	3.00
			High input concentration (300 μM)				
			Observations				
Mean	0.681	1.41	4.76	3.56	0	0	15.0
±SD	0.116	0.48	0.89	0.96			4.43
			Simulations				
Model							
AEDCCA	0.816	1.44	4.25	2.95	5.27	15.6	7.09
AEECCA	0.813	1.43	4.28	3.21	4.77	14.1	6.16
BCACCA	0.814	1.45	4.28	2.96	4.83	14.2	5.95
CAACCA	0.812	1.43	4.59	3.20	4.55	13.4	5.60
CAECCA	0.815	1.44	4.26	2.96	5.07	15.0	6.55

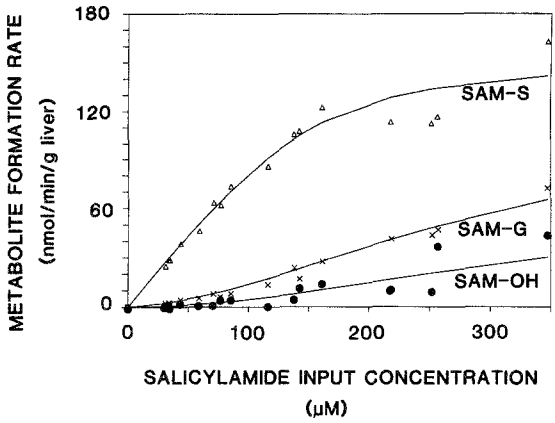

Fig. 4. Predicted *versus* observed formation rates of SAM metabolites. K_m's of 15, 180, and 280 μM and V_{max}'s of 1546, 1400, and 887 nmol/min for SAM sulfation, glucuronidation, and hydroxylation, respectively (from Ref. 17), were used in Model CAECCA to predict (solid line) SAM metabolite formation rates with SAM input concentrations varied from 30 to 350 μM in once-through perfused rat livers (data from Ref. 17). The symbols are observations for rates of formation of SAM-S (△), SAM-G(×), and (total) hydroxylated metabolites (●), SAM-OH.

without the addition of DCNP (17). The results obtained from the simulation study (Model CAECCA) were compared with observed data (Figs. 4 and 5); simulated data with Model AEDCCA matched the observations equally well (data not shown).

DISCUSSION

Normal and retrograde rat liver perfusions and simulations of enzyme distribution models have been utilized in the present investigation to examine and possibly explain the drastically dissimilar metabolic fates between preformed and generated GAM. By changing the perfusion flow direction, recruitment of drug metabolizing enzyme activities occurs in a reverse fashion and any inherent heterogeneity in enzymic activity will be readily revealed by an increased or decreased formation of metabolites. The lower input (134 μM) concentration exceeds the apparent K_m (K_m/unbound fraction of SAM) for SAM sulfation but not for glucuronidation and hydroxylation. The higher input (295 μM) concentration exceeds

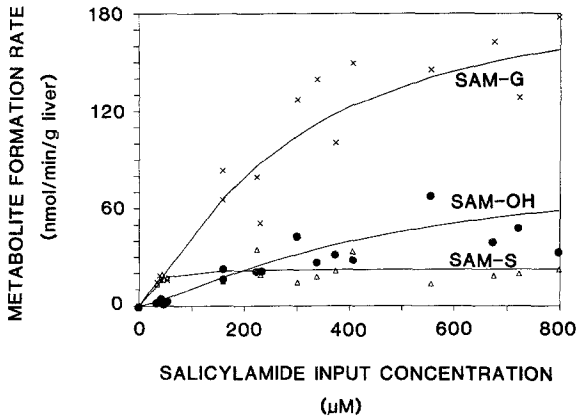

Fig. 5. Predicted *versus* observed formation rates of SAM metabolites. K_m's of 4.7, 150, and 280 μM and V_{max}'s of 226, 2000, and 887 nmol/min for SAM sulfation, glucuronidation, and hydroxylation, respectively (from Ref. 17), were used in Model CAECCA to predict (solid line) SAM metabolite formation rates with SAM input concentration varied from 33 to 800 μM in the presence of 40 μM DCNP, a sulfation inhibitor. The symbols are observations for rates of formation of SAM-S (△), SAM-G (×) and (total) hydroxylated metabolites (●), SAM-OH.

the apparent K_m's for SAM sulfation and glucuronidation but not for SAM hydroxylation. As shown theoretically (2) and experimentally for harmol (12) and GAM (5), both input conditions would render metabolite formation ratios discriminatory and point toward the relative enzyme distribution patterns in SAM metabolism, as shown for GAM metabolism (6). The lower concentration, however, should provide a larger difference in metabolite ratio between N and R perfusion (data in Table III).

Results from liver perfusion experiments indicated that at the lower input SAM concentration, small and variable amounts of SAM hydroxylated metabolites were formed, causing large variations in the metabolic formation ratio, SAM-S/SAM-OH. The variability reduced the sensitivity of this metabolite formation ratio as an indicator to detect the zonal heterogeneities of enzymes involved. Instead, at the higher input concentration (295 μM), significant changes in the ratios of SAM-S/SAM-G and SAM-S/SAM-OH between N and R perfusion were observed.

As expected of an anterior sulfation system in relation to the glucuronidation system, the ratio of metabolic rates, SAM-S/SAM-G, decreased during R compared to N ($p < 0.05$) for both SAM concentrations studied.

The statistically significant decrease in the ratio of SAM-S/SAM-OH was observed only at the higher input SAM concentration. These observations are also attributed to a strong SAM sulfation but poor hydroxylation activities. Differences in SAM-G/SAM-OH during N and R were small at both SAM C_{In}'s and are perhaps due to the close proximities of the enzyme systems. The lack of change in SAM hydroxylation rate during both N and R at the high C_{In} is not unexpected because it is a poor metabolic pathway. Based on these findings, the relative enzyme distribution patterns may be assigned: an anterior enzymic distribution for sulfation and posterior localizations for SAM glucuronidation and hydroxylation.

Computer simulations (SAM parallel model) further supported these distribution patterns, with Model CAE giving the smallest WSSR, while other models, whose median distances for sulfation, glucuronidation, and hydroxylation activities are of the same rank order as in Model CAE, also predicted the data, albeit with increased WSSR. These relative enzymic distributions of the models were in general agreement with those found by others on sulfation and glucuronidation (3–5, 8, 22–25). Our pattern on SAM hydroxylation activity is also similar to those found for cytochrome P-450-mediated reaction, phenacetin *O*-deethylation (14–16), benzo(*a*)pyrene hydroxylation (26), 7-ethoxycoumarin *O*-deethylation (27), and lidocaine hydroxylation (28), and by immunohistochemical and staining on the localization and distribution of phenobarbital- and 3-methylcholantrene inducible cytochromes P-450 (29–31).

In the expanded modeling on parallel-sequential pathways, the sequential metabolism of SAM (conjugation of the primary metabolite, GAM) was also considered. Two models (CAECCA and AEDCCA) were selected, with SAM hydroxylation activities localized perivenularly and GAM glucuronidation activities being evenly distributed and regionalized in a manner which should favor GAM glucuronidation over GAM sulfation (more anteriorly distributed). For CAECCA, sulfation activities for SAM and GAM are identically distributed (more periportal) as are SAM and GAM glucuronidation (evenly distributed) activities. Despite these models being selected as the best models based on the criteria of WSSR and ADIF, the simulated data failed to predict the exclusive glucuronidation of GAM. Rather, they predicted GAM sulfations (forming GAM-2S and GAM-5S) as the major metabolic pathways of GAM inasmuch as the low K_m's and the overlap of enzymes for SAM hydroxylation and GAM sulfation. Failure of the models adequately to predict GAM conjugation is perhaps due to the modeling approaches. Although a distributed-in-space phenomenon is described for drug and metabolite processing, the tissue (hepatocyte) is viewed as a single well-mixed compartment, without further consideration

of subcompartmentalization of cellular structures. That is, enzymes distributed in both cytosol and endoplasmic reticulum are considered to be equally accessible to substrates or metabolites intracellularly. It is likely that subcompartmentalization of structures needs to be considered in modeling for a better prediction of metabolic events. Hydroxylation and glucuronidation, reactions mediated by membrane-bound enzymes, may be more coupled compared to those for hydroxylation and sulfation (32,33). In view of these subcellular locations of enzyme systems, GAM, once formed, will immediately undergo glucuronidation to form GAM-5G before being released to the cytosol for sulfation to occur. Therefore, the likelihood of sulfoconjugation of GAM is relatively lower than those predicted from the present modeling. This work brings attention to further refinement on the modeling of enzymic distributions in the processing of drugs and metabolites in the liver.

APPENDIX A

Differential Equations to Describe SAM Disappearance and SAM Metabolite Formation from Competing Pathways (Parallel Model).

Based on mass balance, the following equations were derived to describe the elimination of SAM and formation of SAM metabolites in the once-through liver perfusion system at steady-state.

Rate of disappearance of SAM:

$$\frac{Q\,dC_x}{dx} = -\frac{1}{L}\left\{\frac{V_{\max,x}^{\text{SAM-S}} C_{u,x}}{K_m^{\text{SAM-S}} + C_{u,x}} + \frac{V_{\max,x}^{\text{SAM-G}} C_{u,x}}{K_m^{\text{SAM-G}} + C_{u,x}} + \frac{V_{\max,x}^{\text{SAM-OH}} C_{u,x}}{K_m^{\text{SAM-OH}} + C_{u,x}}\right\} \quad \text{(A1)}$$

Rate of formation of SAM-S:

$$\frac{Q\,dC_x^{\text{SAM-S}}}{dx} = \frac{1}{L}\left\{\frac{V_{\max,x}^{\text{SAM-S}} C_{u,x}}{K_m^{\text{SAM-S}} + C_{u,x}}\right\} \quad \text{(A2)}$$

Rate of formation of SAM-G:

$$\frac{Q\,dC_x^{\text{SAM-G}}}{dx} = \frac{1}{L}\left\{\frac{V_{\max,x}^{\text{SAM-G}} C_{u,x}}{K_m^{\text{SAM-G}} + C_{u,x}}\right\} \quad \text{(A3)}$$

Rate of hydroxylation (formation of GAM):

$$\frac{Q\,dC_x^{\text{SAM-OH}}}{dx} = \frac{1}{L}\left\{\frac{V_{\text{max},x}^{\text{SAM-OH}} C_{\text{u},x}}{K_m^{\text{SAM-OH}} + C_{\text{u},x}}\right\} \tag{A4}$$

where C_x and $C_{\text{u},x}$ are the total and unbound concentrations of SAM in sinusoidal blood at point x, respectively. $C_{\text{u},x}$ also equals the tissue unbound concentration at point x. The superscripts on the concentration terms denote the species considered.

APPENDIX B

Differential Equations to Describe GAM and GAM Conjugate Formation After SAM Perfusion into the Rat Liver (Parallel-Sequential Model)

For GAM:

$$\frac{Q\,dC_x^{\text{GAM}}}{dx} = \frac{1}{L}\left\{\frac{V_{\text{max},x}^{\text{SAM-OH}} C_{\text{u},x}}{K_m^{\text{SAM-OH}} + C_{\text{u},x}} - \frac{V_{\text{max},x}^{\text{GAM-2S}} C_x^{\text{GAM}}}{K_m^{\text{GAM-2S}}/f_{\text{B}}\{mi\} + C_x^{\text{GAM}}} - \frac{V_{\text{max},x}^{\text{GAM-5S}} C_x^{\text{GAM}}}{K_m^{\text{GAM-5S}}/f_{\text{B}}\{mi\} + C_x^{\text{GAM}}} - \frac{V_{\text{max},x}^{\text{GAM-5G}} C_x^{\text{GAM}}}{K_m^{\text{GAM-5G}}/f_{\text{B}}\{mi\} + C_x^{\text{GAM}}}\right\} \tag{B1}$$

For GAM-2S:

$$\frac{Q\,dC_x^{\text{GAM-2S}}}{dx} = \frac{1}{L}\left\{\frac{V_{\text{max},x}^{\text{GAM-2S}} C_x^{\text{GAM}}}{K_m^{\text{GAM-2S}}/f_{\text{B}}\{mi\} + C_x^{\text{GAM}}}\right\} \tag{B2}$$

For GAM-5S:

$$\frac{Q\,dC_x^{\text{GAM-5S}}}{dx} = \frac{1}{L}\left\{\frac{V_{\text{max},x}^{\text{GAM-5S}} C_x^{\text{GAM}}}{K_m^{\text{GAM-5S}}/f_{\text{B}}\{mi\} + C_x^{\text{GAM}}}\right\} \tag{B3}$$

For GAM-5G:

$$\frac{Q\,dC_x^{\text{GAM-5G}}}{dx} = \frac{1}{L}\left\{\frac{V_{max,x}^{\text{GAM-5G}} C_x^{\text{GAM}}}{K_m^{\text{GAM-5G}}/f_{\text{B}}\{mi\} + C_x^{\text{GAM}}}\right\} \tag{B4}$$

where C_x and $C_{\text{u},x}$ are the total and unbound sinusoidal concentrations of SAM; and C_x^{GAM}, $C_x^{\text{GAM-2S}}$, $C_x^{\text{GAM-5S}}$, and $C_x^{\text{GAM-5G}}$ denote the total

sinusoidal concentrations of GAM, GAM-2S, GAM-5S, and GAM-5G at point x, respectively; $f_B\{mi\}$ denotes the unbound fraction in blood for GAM.

REFERENCES

1. K. S. Pang, X. Xu, M. E. Morris, and V. Yuen. Kinetic modeling of conjugations in liver. *Fed. Proc.* **46:**2439-2441 (1987).
2. M. E. Morris and K. S. Pang. Competition between two enzymes for substrate removal in liver: Modulating effects due to substrate recruitment of hepatocyte activity. *J. Pharmacokin. Biopharm.* **15:**473-496 (1987).
3. K. S. Pang, H. Koster, I. C. M. Halsema, E. Scholtens, G. J. Mulder, and R. N. Stillwell. Normal and retrograde perfusion to probe the zonal distribution of sulfation and glucuronidation activities of harmol in the perfused rat liver preparation. *J. Pharmacol. Exp. Ther.* **224:**647-653 (1983).
4. J. R. Dawson, J. G. Weitering, G. J. Mulder, R. N. Stillwell, and K. S. Pang. Alteration of transit time and direction of flow to probe the heterogeneous distribution of conjugating activities for harmol in the perfused rat liver preparation. *J. Pharmacol. Exp. Ther.* **234:**691-697 (1985).
5. M. E. Morris, V. Yuen, and K. S. Pang. Competing pathways in drug metabolism. II. An identical, anterior enzymic distribution for 2- and 5-sulfoconjugation and a posterior localization for 5-glucuronidation of gentisamide in the rat liver. *J. Pharmacokin. Biopharm.* **16:**633-656 (1988).
6. M. E. Morris, V. Yuen, B. K. Tang, and K. S. Pang. Competing pathways in drug metabolism. I. Effect of input concentration on the conjugation of gentisamide in the once-through *in situ* perfused rat liver preparation. *J. Pharmacol. Exp. Ther.* **245:**614-624 (1988).
7. J. G. Conway, F. C. Kauffman, S. Ji, and R. G. Thurman. Rates of sulfation and glucuronidation of 7-hydroxycoumarin in periportal and pericentral regions of the liver lobule. *Mol. Pharmacol.* **22:**509-516 (1982).
8. J. G. Conway, F. C. Kauffman, T. Tsukuda, and R. G. Thurman. Glucuronidation of 7-hydroxycoumarin in periportal and pericentral regions of the lobule in livers from untreated and 3-methylcholanthrene-treated rats. *Mol. Pharmacol.* **33:**111-119 (1988).
9. S. Orrenius, B. Andersson, B. Jernstrom, and P. Moldéus. Isolated hepatocytes as an experimental tool in the study of drug conjugation reactions. In A. Aitio (ed.), *Conjugation Reactions in Drug Biotransformation*, Elsevier, Amsterdam, 1978, pp. 273-282.
10. M. Koike, K. Sugeno, and M. Hirata. Sulfoconjugatijon and glucuronidation of salicylamide in isolated rat hepatocytes. *J. Pharm. Sci.* **70:**308-311 (1981).
11. K. S. Pang, P. Kong, J. A. Terrell, and R. E. Billings. Metabolism of acetaminophen and phenacetin by isolated rat hepatocytes. A system in which the spatial organization inherent in the liver is disrupted. *Drug Metab. Dispos.* **13:**42-50 (1985).
12. K. S. Pang and R. N. Stillwell. An understanding of the role of enzymic localization of the liver on metabolite kinetics: A computer simulation. *J. Pharmacokin. Biopharm.* **11:**451-468 (1983).
13. K. S. Pang. The effects of intercellular distribution of drug metabolizing enzymes on the kinetics of stable metabolite formation and elimination by liver: First-pass effects. *Drug Metab. Rev.* **14:**61-76 (1983).
14. K. S. Pang and J. R. Gillette. Kinetics of metabolite formation and elimination in the perfused rat liver preparation: Differences between the elimination of preformed acetaminophen and acetaminophen formed from phenacetin. *J. Pharmacol. Exp. Ther.* **207:**178-194 (1978).
15. K. S. Pang and J. A. Terrell. Retrograde perfusion to probe the heterogeneous distribution of hepatic drug metabolizing enzymes in rats. *J. Pharmacol. Exp. Ther.* **216:**339-346 (1981).

16. K. S. Pang, W. F. Cherry, J. Accaputo, A. J. Schwab, and C. A. Goresky. Combined hepatic arterial-portal venous or hepatic venous flows once-through the *in situ* perfused rat liver to probe the abundance of drug metabolizing activities. Perihepatic venous O-deethylation activity for phenacetin and periportal sulfation activity for acetaminophen. *J. Pharmacol. Exp. Ther.* **247:**690–700 (1988).
17. X. Xu, B. K. Tang, and K. S. Pang. Sequential metabolism of salicylamide exclusively to gentisamide-5-glucuronide and not gentisamide sulfate conjugates in the single-pass perfused rat liver. *J. Pharmacol. Exp. Ther.* (under revision).
18. X. Xu and K. S. Pang. Gentisamide metabolism in perfused rat liver preparation: As a generated metabolite of salicylamide and as a preformed metabolite. *Pharmacologist* **28:**Abstr. No. 157 (1986).
19. X. Xu and K. S. Pang. On the estimation of enzymatic parameters with nonlinear protein binding and heterogeneity of drug metabolizing enzymes. *J. Pharmacokin. Biopharm.* (submitted).
20. H. G. Mandel, V. V. Rodwell, and P. K. Smith. A study of the metabolism of C^{14} salicylamide in the human. *J. Pharmacol. Exp. Ther.* **106:**433–439 (1952).
21. X. Xu and K. S. Pang. High-performance liquid chromatographic method for the quantitation of salicylamide and its metabolites in biological fluids. *J. Chromatogr.* **420:**313–327 (1987).
22. J. R. deBaun, J. Y. R. Smith, E. C. Miller, and J. A. Miller. Reactivity *in vivo* of the carcinogen N-hydroxy-2-acetylaminofluorene: Increase by sulfate ion. *Science* **167:**184–186 (1970).
23. J. H. N. Meerman and G. J. Mulder. Prevention of the hepatotoxic action of N-hydroxy-2-acetylaminofluorene in the rat by inhibition of N-O-sulfation by pentachlorophenol. *Life Sci.* **28:**2361–2365 (1981).
24. D. Ullrich, G. Fischer, N. Katz, and K. W. Bock. Intralobular distribution of UDP-glucuronosyltransferase in livers from untreated, 3-methylcholanthrene and phenobarbital-treated rats. *Chem. Biol. Interact.* **48:**181–190 (1984).
25. J. R. Chowdhury, P. M. Novikoff, N. R. Chowdhury, and A. B. Novikoff. Distribution of UDP-glucuronosyltransferase in rat liver. *Proc. Natl. Acad. Sci. USA* **82:**2990–2994 (1985).
26. L. W. Wattenberg and J. L. Leong. Histochemical demonstration of reduced pyridine nucleotide dependent polycyclic hydrocarbon metabolizing systems. *J. Histochem. Cytochem.* **10:**412–420 (1962).
27. S. A. Belinsky, F. C. Kauffman, and R. G. Thurman. Reducing equivalents for mixed function in periportal and pericentral regions of the liver lobule in perfused livers from normal and phenobarbital-treated rats. *Mol. Pharmacol.* **26:**574–581 (1984).
28. K. S. Pang, J. A. Terrell, S. D. Nelson, K. F. Feuer, M.-J. Clements, and L. Endrenyi. An enzyme-distributed system for lidocaine metabolism in perfused rat liver preparation. *J. Pharmacokin. Biopharm.* **14:**107–130 (1986).
29. J. Baron, J. A. Redick, and F. P. Guengerich. Immunohistochemical localizations of cytochrome P-450 in the rat liver. *Life Sci.* **23:**2627–2632 (1978).
30. J. Baron, J. A. Redick, and F. P. Guengerich. An immunohistochemical study on the localizations and distributions of phenobarbital- and 3-methylcholantrene-inducible cytochrome P-450 within the livers of untreated rats. *J. Biol. Chem.* **256:**5931–5937 (1981).
31. P. E. Gooding, J. Chayen, B. Sawyer, and T. F. Slater. Cytochrome P-450 distribution in rat liver and the effect of sodium phenobarbitone administration. *Chem.-Biol. Interact.* **20:**299–310 (1978).
32. J. W. DePierre and G. Dallner. Structural aspects of the membrane of the endoplasmic reticulum. *Biochim. Biophys. Acta* **415:**411–472 (1975).
33. J. W. DePierre, G. Andersson, and G. Dallner. Endoplasmic reticulum and golgi complex. In I. M. Arias (ed.), *The Liver: Biology and Pathobiology*, Raven Press, New York, 1988, pp. 165–187.